Synthetic Metals 271 (2021) 116636

Contents lists available at ScienceDirect

Synthetic Metals

journal homepage: www.elsevier.com/locate/synmet

Research paper

Effects of the indium tin oxide/perovskite interface on the photocurrent amplification of perovskite photodetectors

Lidan Wang [a], Zisheng Su [b,*], Hairuo Wu [c,d], Bei Chu [c]

[a] College of Chemical Engineering and Material, Quanzhou Normal University, Quanzhou 362000, PR China
[b] College of Physics and Information Engineering, Key Laboratory of Information Functional Material for Fujian Higher Education and Fujian Key Laboratory for Advanced Micro-nano Photonics Technology and Devices, Quanzhou Normal University, Quanzhou 362000, PR China
[c] State Key Laboratory of Luminescence and Applications, Changchun Institute of Optics, Fine Mechanics and Physics, Chinese Academy of Sciences, Changchun 130033, PR China
[d] University of Chinese Academy of Sciences, Beijing 100039, PR China

ARTICLE INFO

Keywords:
Perovskite photodetector
Photocurrent amplification
Inverted structure
Interface

ABSTRACT

Perovskite photodetectors processing a photocurrent amplification have attracted much attention due to their high response to light illumination and have been exploited in a regular device geometry. Here, photocurrent amplification is demonstrated in an inverted perovskite photodetector, and the effect of the indium tin oxide (ITO)/perovskite interface on the photocurrent amplification factor are exploited. It is found that the photocurrent amplification is limited by the ITO/perovskite interface, which can be proved by the devices with bare ITO, Cu_2O particles partially covered ITO, and poly(3,4-ethylene dioxythiophene):poly(styrene sulfonate) fully covered ITO as the anodes. A photocurrent amplification factor of about 27 is demonstrated in the perovskite photodetector with a bare ITO as the anode, which is one of the highest ones among the reported perovskite photodetectors. It also exhibits a maximum response of 4.1 A/W and a detectivity of 10^{11} Jones. Compared with the bare ITO device, the photocurrent amplification of the devices decreases gradually with the reduced contact area between ITO and perovskite and eventually disappears when the direct contact is totally removed. The photocurrent amplification is attributed to the long-lived accumulated holes as well as the positively charged $CH_3NH_3^+$ and I vacancy at the ITO/perovskite interface, which dramatically lowers the injection barrier of electrons and leads to a multiple electron injection.

1. Introduction

Organic/inorganic hybrid perovskites such as $CH_3NH_3PbI_3$ have attracted tremendous attention for applications in the fields of solar cells and light-emitting diodes because of their direct bandgap, high absorption coefficient, long exciton diffusion length, and excellent charge transport property [1–5]. Photodetector is another important type of optoelectronic devices which has been widely utilized in optical communication, imaging, environmental monitoring, and chemical/biological sensing. Organic/inorganic hybrid perovskite has been considered to be one of the ideal materials for photodetectors owing to their merits of high defect tolerance and long carrier lifetime. Taking advantage of these superior properties, high performance perovskite photodetectors have been realized in recent years [6–15]. There are generally two typical device structures for perovskite photodetectors, e.g., photodiode- and photomultiplication-photodetectors. For the photodiode-type photodetectors, the maximum external quantum efficiency (EQE) is lower than 100%, while for the photomultiplication-type ones it is dramatically higher than 100%, indicating that a photocurrent amplification realized in these devices. The photocurrent amplification is triggered on that one type of charge carriers can travel across the device several times before they recombined with the opposite charge carriers that trapped in the devices [16]. Thus a high density of charge traps is required in the device for the photomultiplication-type photodetectors. Owing to the long charge carrier lifetime in perovskite, photomultiplication perovskite photodetectors have gained increased attention in recent year [17–25]. The trapped charge carriers can be holes or electrons. For example, Dong et al. demonstrated a photocurrent amplification when a higher content of PbI_2 was added in the precursor solution due to the excess Pb^{2+} at the top surface of perovskite

* Corresponding author.
E-mail address: suzs@qztc.edu.cn (Z. Su).

https://doi.org/10.1016/j.synthmet.2020.116636
Received 31 July 2020; Received in revised form 9 November 2020; Accepted 16 November 2020
Available online 23 November 2020
0379-6779/

can act as the hole traps [18], and Ishii et al. proved that holes can be accumulated at the perovskite/Eu complex interface with a suitable energy level alignment [25]. In contrast, Liu et al. reported that PbS quantum dots in perovskite can act as electron traps [21], and Zhang et al. found that small molecular organic material can also sever as the electron traps when it was doped in the electron-transporting layer [24]. More interesting, it is found that photocurrent amplification can be found when the perovskite film contacts directly with the bottom FTO cathode but without the need of artificial charge carrier traps [17,19]. However, the mechanisms are still under debating. For example, Moehl et al. proposed that the photocurrent amplification is attributed to the ion migration in perovskite [20], while Chen et al. suggested that it is relays on the ferroelectric property of the perovskite [19].

In this work, we demonstrated a photocurrent amplification in an inverted perovskite photodetector with $CH_3NH_3PbI_3$ directly contacting with indium tin oxide (ITO) anode, and the effect of the ITO/perovskite interface on the photocurrent amplification factor of the perovskite photodetectors are investigated. It is found that the photocurrent amplification factor, which defined as the ratio between the photocurrent at a given negative voltage and the one at 0 V, decreases with the decrease of the contact area between ITO and $CH_3NH_3PbI_3$ when Cu_2O particles were deposited on ITO as the blockers, and it completely disappears when the contact area is fully removed by a poly(3,4-ethylene dioxythiophene):poly(styrene sulfonate) (PEDOT:PSS) spacer layer. This work demonstrates that photocurrent amplification can be obtained in an inverted hole-transporting layer (HTL)-free perovskite photodetector in addition to the reported regular devices with a bottom transparent conductive oxide as the cathode, and a mechanism is proposed for this photocurrent amplification.

2. Experimental details

The perovskite photodetector has a structure of ITO/$CH_3NH_3PbI_3$/C_{60} (40 nm)/4,7-diphenyl-1,10-phenanthroline (Bphen, 8 nm)/Ag (100 nm), as shown in Fig. 1(a). ITO coated grass with a sheet resistance of 15 Ω/sq was used as the substrate, and it was routinely cleaned followed by UV-ozone treatment for 15 min. $CH_3NH_3PbI_3$ layer was deposited with a two-step solution process in ambient conditions [26]. PbI_2 which dissolved in N,N-dimethylformamide with a concentration of 460 mg/ml was first spin-coated on the ITO substrate at 2000 rpm for 30 s, and followed by annealing at 70 ℃ for 5 min. Then CH_3NH_3I dissolved in isopropanol with a concentration of 50 mg/ml was spin-coated on the PbI_2 film at 2000 rpm for 30 s and followed by annealing at 100 ℃ for 1 h, which formed a $CH_3NH_3PbI_3$ layer directly on the ITO substrate. Finally, 40 nm C_{60}, 8 nm Bphen, and 100 nm of Ag were sequentially thermally evaporated on the perovskite layer at a pressure of 5×10^{-4} Pa. The deposition rate and layer thickness were monitored *in situ* using oscillating quartz monitors, and the deposition rates were kept at 1 Å/s for C_{60} and Bphen and 5 Å/s for Ag cathode.

For reference, photodetectors on Cu_2O particles partially covered ITO substrates and PEDOT:PSS fully covered ITO substrate were also constructed. The Cu_2O particles were deposited on ITO with an electrodeposited method [27,28]. An alkaline aqueous solution containing 0.3 M copper sulfate and 3 M lactic acid with a pH value of 12 that adjusted by sodium hydroxide was used as the precursor. The deposition was carried out in a configured glass cell at 70 ℃, in which the ITO substrate, a platinum plate, and an Ag/AgCl electrode in a saturated KCl solution served as the working electrode, the counter electrode, and the reference electrode, respectively. During the electrodeposition, the potential was set to be −0.5 V, and the current densities observed during the deposition ranged from 1 to 1.2 mA/cm^2. The duration of the deposition was 20 and 30 s, which formed Cu_2O particles with a lower and a higher densities on ITO substrates, respectively. Finally the substrates were rinsed with deionized water and dried in air naturally. PEDOT:PSS (Clevios P-VP Al4083) was filtered and deposited onto ITO substrate through spin-coating at 4000 rpm for 40 s, and then annealed at 120 °C for 15 min in ambient conditions, which forms a PEDOT:PSS layer of about 40 nm.

The morphology of the perovskite films were measured by a Hitachi S4800 field emission scanning electron microscopy (SEM), and the Cu_2O particles were measured by a Philips-FEI XL30-SFEG SEM. X-ray diffraction (XRD) pattern was obtained with a Rigaku D/Max-2500 diffractometer using Cu Kα radiation (λ = 1.54 Å). Absorption spectrum was recorded on a Lambda 900 spectrophotometer. Current-voltage (J-V) characteristics of the devices were measured with a Keithley 2400 source meter both in dark and under illumination of a Xe lamp light source with an AM 1.5 G filter, and the irradiation intensity was certified to be of 100 mW/cm^2. The EQE spectrum was performed with a Stanford SR 830 lock-in amplifier under monochromatic illumination. All measurements were performed under ambient conditions.

3. Results and discussions

Fig. 1(b) and (c) show the top-view and cross-sectional SEM images of the $CH_3NH_3PbI_3$ film on a bare ITO substrate, respectively. A compact and pin-hole free morphology is found for the $CH_3NH_3PbI_3$ film, and the grain size is about 200–300 nm. Such a compact morphology eliminates short-circuit between the bottom ITO anode and the upper Ag cathode even no HTL were adopted here. The thickness of the $CH_3NH_3PbI_3$ film obtained from the cross-sectional SEM image is about 300 nm. Besides, the $CH_3NH_3PbI_3$ film displays high characteristic diffraction peaks of 2θ at about 14.16° and 28.50° (Fig. S1), which can be assigned to the diffraction of the (110) and (220) planes of $CH_3NH_3PbI_3$, respectively. Meanwhile, low intensity diffraction peaks of PbI_2 can also be found in the XRD pattern, which indicates that a small amount of unrecated PbI_2 retains in the perovskite film. Such unrecated PbI_2 may act as hole traps and triggers photocurrent amplification of the device [18]. The $CH_3NH_3PbI_3$ film reveals a broad absorption band at visible region with an edge at about 780 nm (Fig. S2a), corresponding to a bandgap of about 1.56 eV calculated from the Tauc plot of the absorption spectrum

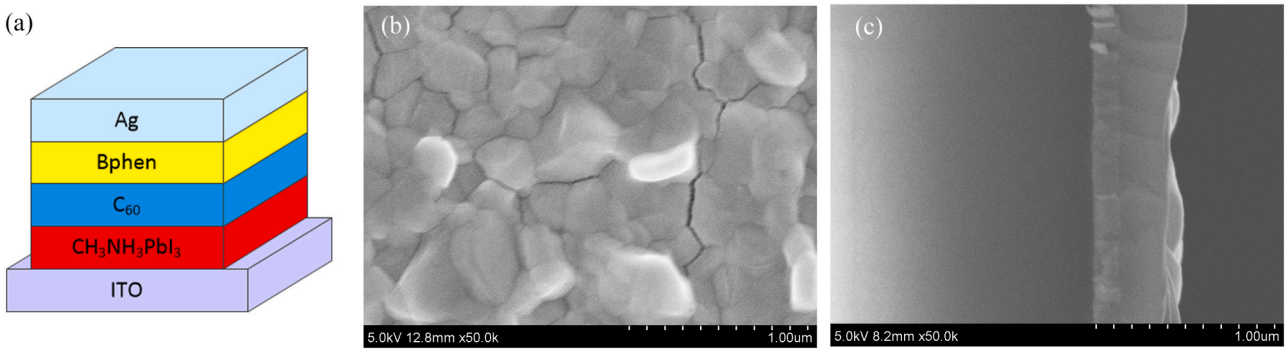

Fig. 1. (a) Device structure of the perovskite photodetector, (b) top-view SEM and (c) cross-sectional SEM of the $CH_3NH_3PbI_3$ film on ITO substrate.

(Fig. S2b). These characters further indicate the formation of a $CH_3NH_3PbI_3$ film on the ITO substrate.

It is reported that the photocurrent amplification in regular perovskite photodetectors is attributed to the direct contact between FTO cathode and the perovskites [17,19,20]. To further understand the effect of the ITO/$CH_3NH_3PbI_3$ interface on the photocurrent amplification in our inverted photodetectors, devices with different anodes were constructed. In our previous works, we have demonstrated that large Cu_2O particles can be deposited on ITO substrates through an electrodeposited method [27,28], which forms a partially covered ITO surface. As shown in Fig. 2(a) and (b), the Cu_2O particles are semisphere with a diameter of about 1–2 μm for an electrodeposition time of 20 and 30 s, and the density of the Cu_2O particles increases with the deposition time. These large Cu_2O particles can partially cover the ITO substrate, decreasing the contact area between ITO and $CH_3NH_3PbI_3$. However, the $CH_3NH_3PbI_3$ films on these Cu_2O particles exhibit dramatically increased grain size to more than 1 μm, as shown in Fig. 2(c) and (d), which is attributed to the manipulated growth process of the perovskite by the Cu_2O particles [28]. Furthermore, we have also fabricated a photodetector on an ITO/PEDOT:PSS anode, which exhibits a fully eliminated contact between ITO and $CH_3NH_3PbI_3$ by using the 40 nm PEDOT:PSS as the spacer. The SEM image of $CH_3NH_3PbI_3$ on PEDOT:PSS is shown in Fig. S3, which reveals a comparable grain size to that on bare ITO.

The J-V curve of the perovskite photodetectors under illumination of an AM 1.5 G solar simulator with an intensity of 100 mW/cm^2 is presented in Fig. 3a. It can be found that the photocurrent dramatically increases with the applied negative voltage for the photodetector on bare ITO anode. The photocurrent at 0 V is 6.04 mA/cm^2, while it reaches 166 mA/cm^2 at −1 V. This corresponds to a photocurrent amplification factor of about 27, which is comparable and even a little higher than the reported regular structure perovskite photodetectors with a direct contact between FTO and the perovskites [17,19]. Meanwhile, both Moehl et al. [17] and Chen et al. [19] demonstrated that the amplification factor can be further increased with a lower illumination intensity, as the photocurrent could not be saturated at higher voltage. Thus a higher amplification factor can be expected with a decreased illumination intensity.

On the other hands, the photodetectors based on Cu_2O particles show a significant increased photocurrent at 0 V, which are 16.8 and 14.7 mA/cm^2 for the low and high densities Cu_2O particles devices, respectively, as shown in Fig. 3a. In contrast, the photocurrents of these devices increase slowly with the applied negative voltage as compared with the device on bare ITO, which are 85.4 and 38.2 mA/cm^2 for the low and high densities Cu_2O particles devices, corresponding to a photocurrent amplification factor only about 5 and 3, respectively. The lower photocurrent of the device with a high Cu_2O particles should be attributed to the increased series resistance due to the introduction of Cu_2O particles [27]. This decreased photocurrent amplification in the Cu_2O particles partially covered ITO devices suggests that the photocurrent amplification of the photodetectors is limited by the contact between ITO and $CH_3NH_3PbI_3$, but not by the morphology of the $CH_3NH_3PbI_3$ films. The photocurrent is further increased to 18.2 mA/cm^2 at 0 V of the photodetector on an ITO/PEDOT:PSS anode, which is attributed to the improved hole collection efficiency with the PEDOT:PSS HTL. However, photocurrent is almost unchanged with the applied negative voltage, indicating that no photocurrent amplification is observed. These findings further confirm that the ITO/$CH_3NH_3PbI_3$ interface plays an important role in determining the photocurrent amplification in these inverted photodetectors.

Fig. 3b displays the dark current of the photodetectors. The dark current is highest for the photodetector on bare ITO and it reduces with the decreased contact area between ITO and $CH_3NH_3PbI_3$. The dark current of the photodetector on PEDOT:PSS is about 4 orders of magnitude lower than that one on bare ITO. This significantly reduced dark current is attributed to the blocked electron injection from ITO to $CH_3NH_3PbI_3$ by the Cu_2O particles or PEDOT:PSS layer. It should be noted that although the dark currents of the devices on Cu_2O particles are lower than that on bare ITO at lower voltage, they are comparable at higher voltage, for example at −1 V. The dark current can be injection-limited and/or transporting-limited. These distinctions between the dark currents indicate that they are injection-limited at lower voltage and the introduction of Cu_2O particles increases the hole injection barrier from ITO to $CH_3NH_3PbI_3$ and hence a lower dark current, while they change to transporting-limited at higher voltage and they exhibit a comparable dark current at higher voltage.

The EQE spectrum of the photodetector based on bare ITO at −1 V is

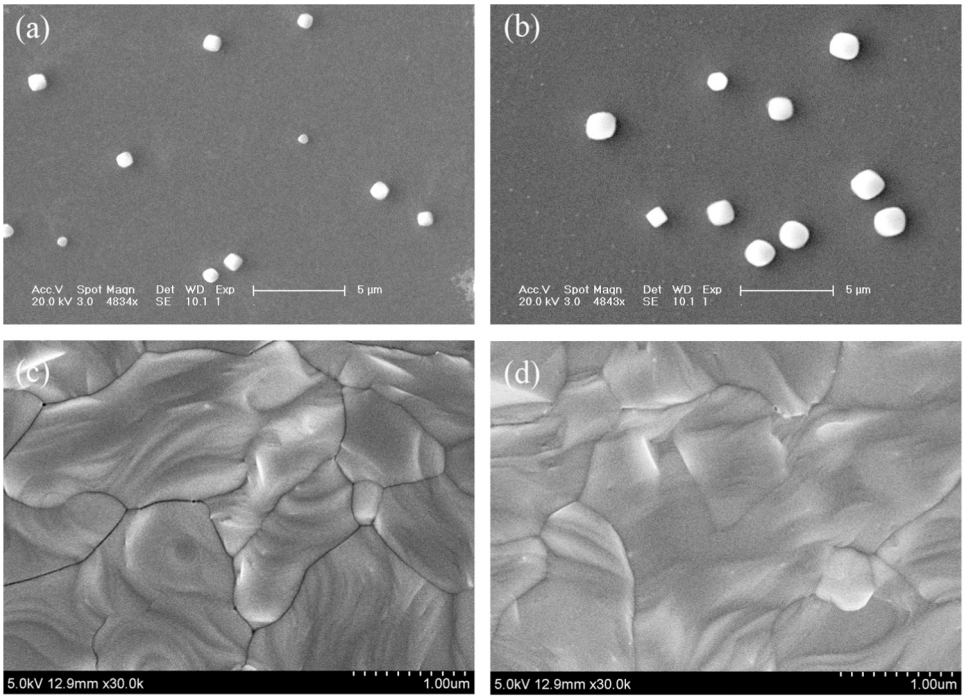

Fig. 2. SEM images of Cu_2O particles with a low (a) and a high (b) densities on ITO substrates, (c) and (d) corresponding $CH_3NH_3PbI_3$ films on these Cu_2O particles.

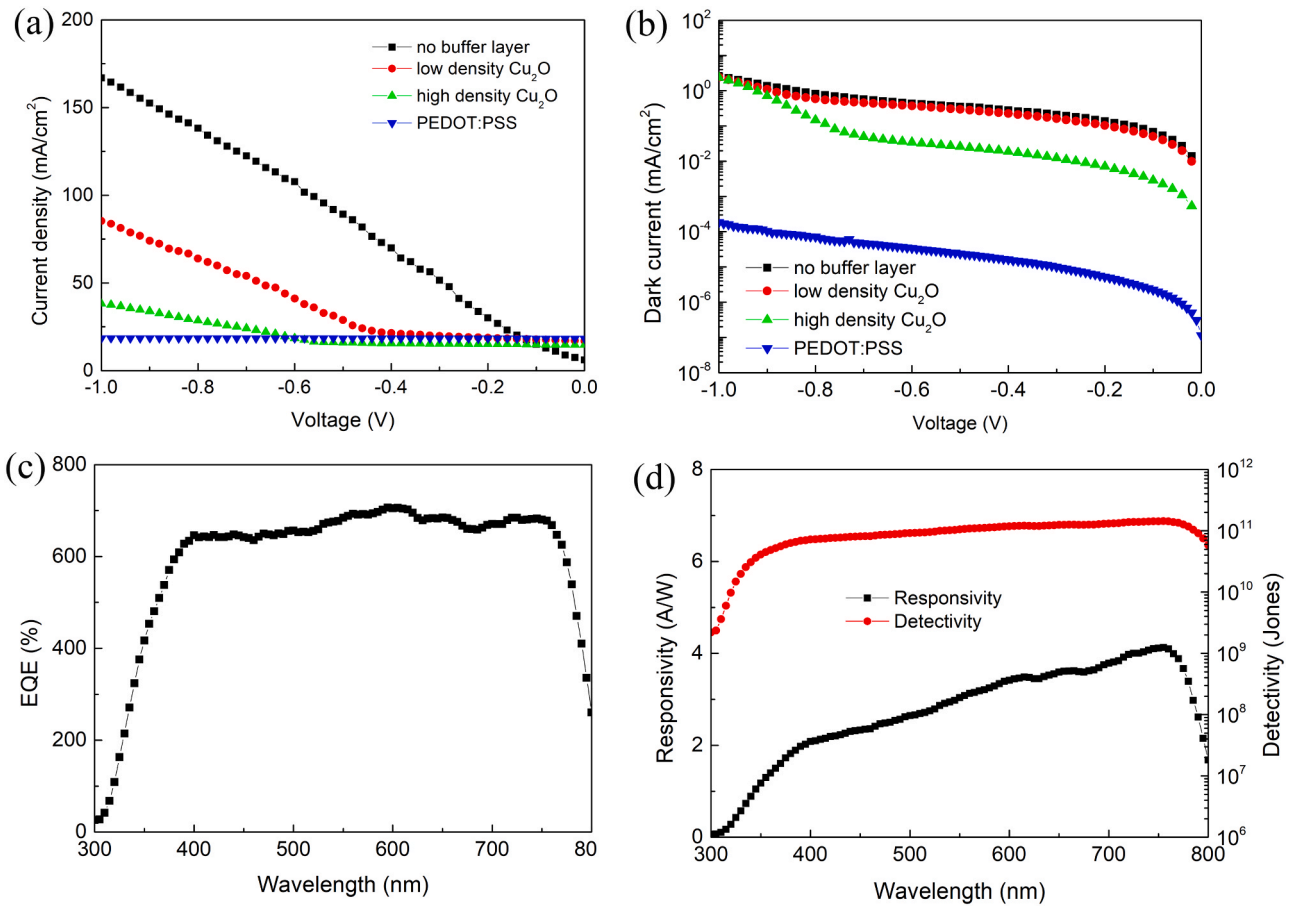

Fig. 3. J-V curves of the photodetectors with different anodes (a) under illumination of an AM 1.5 G solar simulator with an intensity of 100 mW/cm^2 and (b) in dark, where no buffer layer indicates a fully contact, the low and high density Cu_2O for partially contact, while the PEDOT:PSS for no contact between ITO and $CH_3NH_3PbI_3$. (c) EQE spectrum (d) responsivity as well as the detectivity of the photodetector on bare ITO at −1 V.

shown in Fig. 3c. The device reveals a broad response in the visible region, and a sharply decreased response is observed at about 780, which is consistent with the absorption spectrum of $CH_3NH_3PbI_3$, suggesting that the photocurrent is originated from the absorption of $CH_3NH_3PbI_3$. A maximum EQE of about 700% is found, which also indicates that a photocurrent gain achieved in this device. Based on this EQE spectrum, the responsivity and detectivity can be calculated [23], as shown in Fig. 3d. A maximum responsivity of 4.1 A/W at 755 nm is obtained. Meanwhile, a detectivity in the order of 10^{11} Jones is found for the photodetector in visible region with a maximum of 1.4×10^{11} Jones at 755 nm. In view of that the detectivity of a photodetector is simultaneously determined by the responsivity and dark current, it can be further increased if the dark current of our devices were decreased.

Based on these findings, a mechanism is proposed for the photocurrent amplification of the inverted HTL-free photodetector, as shown in Fig. 4. The work function of ITO is 4.72 eV [29], while it is 4.65 eV for $CH_3NH_3PbI_3$ [30]. Thus a downward shift energy level at the ITO/$CH_3NH_3PbI_3$ interface can be anticipated due to the electron transfer from $CH_3NH_3PbI_3$ to ITO (Fig. 4b). The highest occupied molecular orbital (HOMO) and the lowest unoccupied molecular orbital (LUMO) of $CH_3NH_3PbI_3$ are 5.45 and 3.82 eV, respectively [30]. According to these energy levels, an electron injection barrier from ITO to $CH_3NH_3PbI_3$ is about 0.9 eV and the dark current under negative bias of the photodetector should be primary contributed from the electron

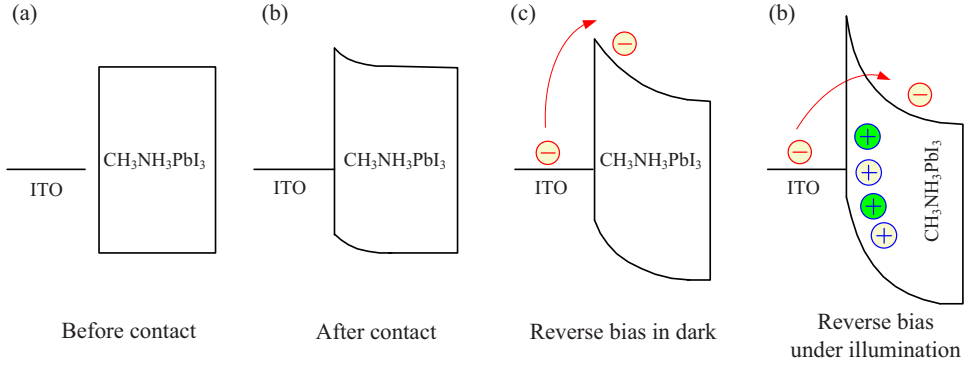

Fig. 4. Schematic mechanism of the photocurrrent amplification in the ITO/$CH_3NH_3PbI_3$/C_{60}/Bphen/Ag photodetectors.

injection because the hole injection barrier from Ag to Bphen is much higher. Thus electrons in ITO should surmount the barrier before they can inject into $CH_3NH_3PbI_3$ (Fig. 4c). Quantum mechanical calculations suggest that there has been a high density of defect states in perovskite films [31]. Thus under illumination photogenerated holes will transport toward ITO anode and then be trapped by the defect states at the ITO/$CH_3NH_3PbI_3$ interface. On the other hand, ions and defects migration in perovskite have been demonstrated by many independent works [32–36]. The migration active energy of $CH_3NH_3^+$ and I vacancy ($V_I^\bullet$) ranges from 0.1 to 1 eV [37–39], and it can be further decreased under illumination [40]. As a result, under illumination and negative bias, $CH_3NH_3^+$ and $V_I^\bullet$ would migrate from the bulk of $CH_3NH_3PbI_3$ to ITO anode and then accumulate at the ITO/$CH_3NH_3PbI_3$ interface. The accumulation of holes as well as the positively charged $CH_3NH_3^+$ and $V_I^\bullet$ leads to a further downward shift energy level at the ITO/$CH_3NH_3PbI_3$ interface (Fig. 4d). Thus the triangle electron injection barrier becomes thinner, which increases the probability for electrons tunneling injection from ITO to $CH_3NH_3PbI_3$, corresponding to a reduced electron injection barrier at the interface. On the other hands, the long-lived trapped holes and positively charged $CH_3NH_3^+$ and $V_I^\bullet$ at the ITO/$CH_3NH_3PbI_3$ interface ensure that electrons can travel across the device several times before recombination. Although similar accumulation of holes as well as positively charged $CH_3NH_3^+$ and $V_I^\bullet$ happens at the PEDOT:PSS/$CH_3NH_3PbI_3$ interface for the photodetector with a PEDOT:PSS HTL, the high electron injection barrier at the ITO/PEDOT:PSS interface hinders the photocurrent amplification.

Through careful analysis of the I-V curves, a slow and a fast increase of currents are found both in dark and under illumination for the HTL-free photodetector, and a transition voltage between these two stages can be obtained. The electron injection barrier can be estimated from this transition voltage [14]. From the I−V curves shown in Fig. 5, the electron injection barrier is estimated to be 0.83 eV in dark, while it is only 0.12 eV under illumination. These injection barrier values are consistent with our proposed mechanism of the photocurrent amplification. Similar current transitions are observed for the photodetectors with Cu_2O partially covered ITO andoes, and the electron injection barrier is estimated to be 0.85 and 0.86 eV in dark for the devices with low and high Cu_2O particles densities, respectively, while they are 0.45 and 0.56 eV under illumination (Fig. S4). The similar electron injection barrier of the photodetectors on bare ITO and Cu_2O particles covered ITO reasonable explains their comparable dark currents at higher voltage. However, the dramatically different electron injection barriers under illumination restrict the photocurrent of the photodetectors on Cu_2O particles covered ITO anodes. The higher electron injection barrier should be attributed to the increased series resistance of the devices due to the introduction of large Cu_2O particles. However, no current transition is observed in the photodetector with a PEDOT:PSS HTL, suggesting that no photocurrent amplification existed in this device.

4. Conclusion

In summary, photocurrent amplification is demonstrated in an inverted HTL-free perovskite photodetector. The photocurrent amplification effect is related to the ITO/perovskite interface, and it decreases with the decrease of the contact area between ITO and perovskite and eventually disappears when direct contact is completely removed. The HTL-free perovskite photodetector exhibits a maximum response of 4.1 A/W and a detectivity of 10^{11} Jones. The photocurrent amplification is attributed to long-lived accumulated holes and positively charged defect states at the ITO/perovskite interface, which dramatically lowers the electron injection barrier. This work demonstrates that the photocurrent amplification also exists in an inverted perovskite photodetector, which may have the potential application in designing and constructing high performance perovskite photodetectors.

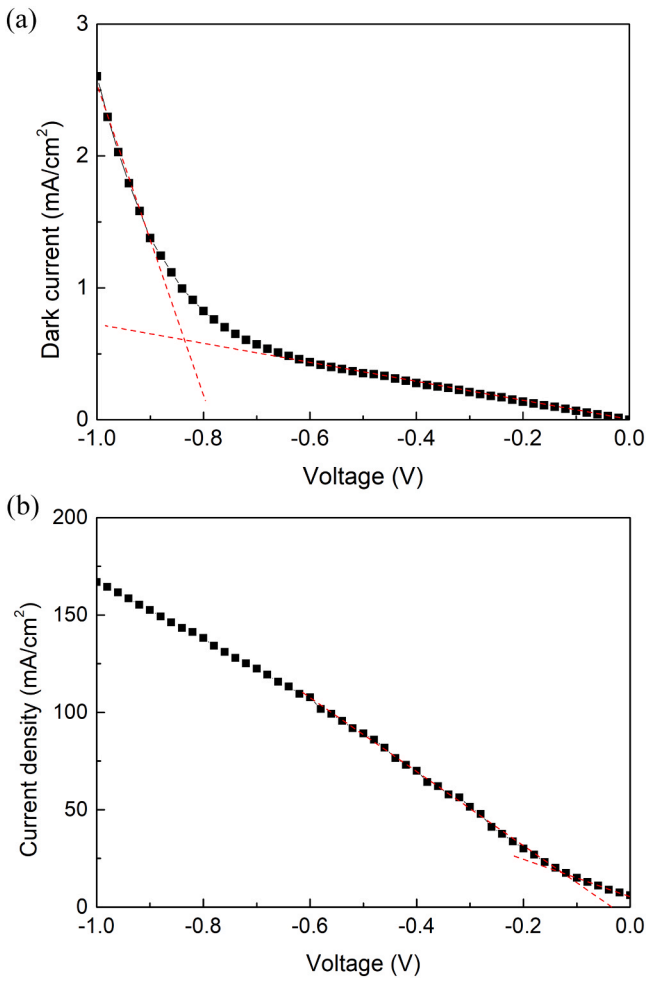

Fig. 5. Extraction of the transition voltages from the currents of the ITO/$CH_3NH_3PbI_3$/C_{60}/Bphen/Ag photodetector (a) in dark and (b) under illumination.

CRediT authorship contribution statement

Lidan Wang: Conceptualization, Methodology, Investigation, Writing - original draft. **Zisheng Su**: Methodology, Writing - review & editing, Supervision. **Hairuo Wu**: Investigation, Visualization. **Bei Chu**: Writing - review & editing.

Declaration of Competing Interest

The authors declare that they have no known competing financial interests or personal relationships that could have appeared to influence the work reported in this paper.

Acknowledgements

This work was supported by the National Natural Science Foundation of China (61504145), the Natural Science Foundation of Fujian Province (2019J01729 and 2020J01778), the Science and Technology Development Plan of Quanzhou (2019C015R and 2020C025R), and the Program for New Century Excellent Talents in Fujian Province University, China.

Appendix A. Supporting information

Supplementary data associated with this article can be found in the online version at doi:10.1016/j.synthmet.2020.116636.

References

[1] A. Kojima, K. Teshima, Y. Shirai, T. Miyasaka, Organometal halide perovskites as visible-light sensitizers for photovoltaic cells, J. Am. Chem. Soc. 131 (2009) 6050–6051.

[2] S.D. Stranks, H.J. Snaith, Metal-halide perovskites for photovoltaic and light-emitting devices, Nat. Nanotechnol. 10 (2015) 391–402.

[3] Q. Jiang, Y. Zhao, X. Zhang, X. Yang, Y. Chen, Z. Chu, Q. Ye, X. Li, Z. Yin, J. You, Surface passivation of perovskite film for efficient solar cells, Nat. Photon. 13 (2019) 460–466.

[4] Y. Cao, N. Wang, H. Tian, J. Guo, Y. Wei, H. Chen, Y. Miao, W. Zou, K. Pang, Y. He, H. Cao, Y. Ke, M. Xu, Y. Wang, M. Yang, K. Du, Z. Fu, D. Kong, D. Dai, Y. Jin, G. Li, H. Li, Q. Peng, J. Wang, W. Huang, Perovskite light-emitting diodes based on spontaneously formed submicrometre-scale structures, Nature 562 (2018) 249–253.

[5] K. Lin, J. Xing, L.N. Quan, F.P.G. de Arguer, X. Gong, J. Lu, L. Xie, W. Zhao, D. Zhang, C. Yan, W. Li, X. Liu, Y. Lu, J. Kirman, E.H. Sargent, Q. Xiong, Z. Wei, Perovskite light-emitting diodes with external quantum efficiency exceeding 20 per cent, Nature 526 (2018) 245–248.

[6] X. Hu, X.D. Zhang, L. Liang, J. Bao, S. Li, W.L. Yang, Y. Xie, High-performance flexible broadband photodetector based on organolead halide perovskite, Adv. Funct. Mater. 24 (2014) 7373–7380.

[7] L.T. Dou, Y. Yang, J.B. You, Z.R. Hong, W.H. Chang, G. Li, Y. Yang, Solution-processed hybrid perovskite photodetectors with high detectivity, Nat. Commun. 5 (2014) 5404.

[8] H. Wu, Z. Su, F. Jin, H. Zhao, W. Li, B. Chu, Improved performance of perovskite photodetectors based on a solution-processed $CH_3NH_3PbI_3/SnO_2$ heterojunction, Org. Electron. 57 (2018) 206–210.

[9] S. Tong, C. Gong, C. Zhang, G. Liu, D. Zhang, C. Zhou, J. Sun, S. Xiao, J. He, Y. Gao, J. Yang, Fully-printed, flexible cesium-doped triple cation perovskite photodetector, Appl. Mater. Today 15 (2019) 389–397.

[10] W. Hu, H. Cong, W. Huang, Y. Huang, L. Chen, A. Pan, C. Xue, Germanium/perovskite heterostructure for high-performance and broadband photodetector from visible to infrared telecommunication band, Light Sci. Appl. 8 (2019) 106.

[11] T. Ji, H. Zhang, N. Han, W. Wang, B. Wu, G. Li, M. Fan, Z. Li, Y. Hao, F. Zhu, Y. Wu, Y. Cui, Plasmonic nanoprism enhanced quasi-2D Ruddlesden-Popper layered perovskite photodetector, J. Mater. Chem. C 8 (2020) 1110–1117.

[12] Y. Dong, Y. Zou, J. Song, X. Song, H. Zeng, Recent progress of metal halide perovskite photodetectors, J. Mater. Chem. C 5 (2017) 11369–11394.

[13] M. Ahmadi, T. Wu, B. Hu, A review on organic-Inorganic halide perovskite photodetectors: device engineering and fundamental physics, Adv. Mater. 29 (2017), 1605242.

[14] P. Wangyang, C. Gong, G. Rao, K. Hu, X. Wang, C. Yan, L. Dai, C. Wu, J. Xiong, Recent advances in halide perovskite photodetectors based on different dimensional materials, Adv. Opt. Mater. 6 (2018), 1701302.

[15] W. Tian, H. Zhou, L. Li, Hybrid organic-inorganic perovskite photodetectors, Small 13 (2017), 1702107.

[16] J. Miao, F. Zhang, Recent progress on highly sensitive perovskite photodetectors, J. Mater. Chem. C 7 (2019) 1741–1791.

[17] T. Moehl, J.H. Im, Y.H. Lee, K. Domanski, F. Giordano, S.M. Zakeeruddin, M.I. Dar, L.-P. Heiniger, M.K. Nazeeruddin, N.-G. Park, M. Grätzel, Strong photocurrent amplification in perovskite solar cells with a porous TiO_2 blocking layer under reverse bias, J. Phys. Chem. Lett. 5 (2014) 3931–3936.

[18] R. Dong, Y. Fang, J. Chae, J. Dai, Z. Xiao, Q. Dong, Y. Yuan, A. Centrone, X.C. Zeng, J. Huang, High-gain and low-driving-voltage photodetectors based on organolead triiodide perovskites, Adv. Mater. 27 (2015) 1912–1918.

[19] H.W. Chen, N. Sakai, A.K. Jena, Y. Sanehira, M. Ikegami, K.C. Ho, T. Miyasaka, A switchable high-sensitivity photodetecting and photovoltaic device with perovskite absorber, J. Phys. Chem. Lett. 6 (2015) 1773–1779.

[20] K. Domanski, W. Tress, T. Moehl, M. Saliba, M.K. Nazeeruddin, M. Gratzel, Working principles of perovskite photodetectors analyzing the interplay between photoconductivity and voltage-driven energy-level alignment, Adv. Funct. Mater. 25 (2015) 6936–6947.

[21] C. Liu, H. Peng, K. Wang, C. Wei, Z. Wang, X. Gong, PbS quantum dots-induced trap-assisted charge injection in perovskite photodetectors, Nano. Energy 30 (2016) 27–35.

[22] J. Yu, X. Chen, Y. Wang, H. Zhou, M. Xue, Y. Xu, Z. Li, C. Ye, J. Zhang, P.A. van Aken, P.D. Lund, H. Wang, A high-performance self-powered broadband photodetector based on a $CH_3NH_3PbI_3$ perovskite/ZnO nanorod array heterostructure, J. Mater. Chem. C 4 (2016) 7302–7308.

[23] Y. Fu, Q. Song, T. Lin, Y. Wang, X. Sun, Z. Su, B. Chu, F. Jin, H. Zhao, W. Li, C. S. Lee, High performance photomultiplication perovskite photodetectors with $PC_{60}BM$ and NPB as the interlayers, Org. Electron. 51 (2017) 200–206.

[24] D. Zhang, C. Liu, K. Li, W. Guo, F. Gao, J. Zhou, X. Zhang, S. Ruan, Trapped-electron-induced hole injection in perovskite photodetector with controllable gain, Adv. Opt. Mater. 6 (2018), 1701189.

[25] A. Ishii, A.K. Jena, T. Miyasaka, Photomultiplying visible light detection by halide perovskite nanoparticles hybridized with an organo Eu complex, J. Phys. Chem. Lett. 10 (2019) 5935–5942.

[26] F. Hou, Z. Su, F. Jin, X. Yan, L. Wang, H. Zhao, J. Zhu, B. Chu, W. Li, Efficient and stable planar heterojunction perovskite solar cells with an MoO_3/PEDOT:PSS hole transporting layer, Nanoscale 7 (2015) 9427–9432.

[27] L. Liu, Z. Su, Q. Xi, G. Gao, W. Yang, Y. Zhao, C. Wu, L. Wang, J. Xu, Trap-assisted large gain in Cu_2O/C_{60} hybrid ultraviolet/visible photodetectors, Appl. Phys. Lett. 108 (2016), 163504.

[28] L. Liu, Q. Xi, G. Gao, W. Yang, H. Zhou, Y. Zhao, C. Wu, L. Wang, J. Xu, Cu_2O particles mediated growth of perovskite for high efficient hole transporting-layer free solar cells in ambient conditions, Sol. Energy Mater. Sol. Cells 157 (2016) 937–942.

[29] Q. Song, T. Lin, X. Sun, B. Chu, Z. Su, H. Yang, W. Li, C.S. Lee, Electronic level alignment at an indium tin oxide/PbI_2 interface and its applications for organic electronic devices, ACS Appl. Mater. Interfaces 10 (2018) 8909–8916.

[30] Y.-F. Chen, Y.-T. Tsai, D.M. Bassani, R. Clerc, D. Forgács, H.J. Bolink, M. Wussler, W. Jaegermann, G. Wantz, L. Hirsch, Evidence of band bending induced by hole trapping at $MAPbI_3$ perovskite/metal interface, J. Mater. Chem. A 4 (2016) 17529–17536.

[31] A. Walsh, D.O. Scanlon, S. Chen, X.G. Gong, S.H. Wei, Self-regulation mechanism for charged point defects in hybrid halide perovskites, Angew. Chem. Int. Ed. 54 (2015) 1791–1794.

[32] Y. Yuan, J. Chae, Y. Shao, Q. Wang, Z. Xiao, A. Centrone, J. Huang, Photovoltaic switching mechanism in lateral structure hybrid perovskite solar cells, Adv. Energy Mater. 5 (2015), 1500615.

[33] Y. Zhao, C. Liang, H. Zhang, D. Li, D. Tian, G. Li, X. Jing, W. Zhang, W. Xiao, Q. Liu, F. Zhang, Z. He, Anomalously large interface charge in polarity-switchable photovoltaic devices: an indication of mobile ions in organic-inorganic halide perovskites, Energy Environ. Sci. 8 (2015) 1256–1260.

[34] T. Leijtens, E.T. Hoke, G. Grancini, D.J. Slotcavage, G.E. Eperon, J.M. Ball, M. D. Bastiani, A.R. Bowring, N. Martino, K. Wojciechowski, M.D. McGehee, H. J. Snaith, A. Petrozza, Mapping electric field-induced switchable poling and structural degradation in hybrid lead halide perovskite thin films, Adv. Energy Mater. 5 (2015), 1500962.

[35] Y. Zhang, M. Liu, G.E. Eperon, T.C. Leijtens, D. McMeekin, M. Saliba, W. Zhang, M. de Bastiani, A. Petrozza, L.M. Herz, M.B. Johnston, H. Lin, H.J. Snaith, Charge selective contacts, mobile ions and anomalous hysteresis in organic-inorganic perovskite solar cells, Mater. Horiz. 2 (2015) 315–322.

[36] T. Wu, M. Ahmadi, B. Hu, Giant current amplification induced by ion migration in perovskite single crystal photodetectors, J. Mater. Chem. C 6 (2018) 8042–8050.

[37] C. Eames, J.M. Frost, P.R.F. Barnes, B.C. O'Regan, A. Walsh, S. Islam, Ionic transport in hybrid lead iodide perovskite solar cells, Nat. Commun. 6 (2015) 7497.

[38] J.M. Azpiroz, E. Mosconi, J. Bisquert, F.D. Angelis, Defect migration in methylammonium lead iodide and its role in perovskite solar cell operation, Energy Environ. Sci. 8 (2015) 2118–2127.

[39] J. Haruyama, K. Sodeyama, L. Han, Y. Tateyama, First-principles study of ion diffusion in perovskite solar cell sensitizers, J. Am. Chem. Soc. 137 (2015) 10048–10051.

[40] Y.-C. Zhao, W.-K. Zhou, X. Zhou, K.-H. Liu, D.-P. Yu, Q. Zhao, Quantification of light-enhanced ionic transport in lead iodide perovskite thin films and its solar cell applications, Light Sci. Appl. 6 (2017), e16243.